Experimental and theoretical study of secondary acoustic instability of downward propagating flames: higher modes and growth rates

Ajit Kumar Dubey, Yoichiro Koyama, Nozomu Hashimoto, and Osamu Fujita.

Division of Mechanical and Space Engineering, Hokkaido University, Kita 13 Nishi 8 Kita-ku, Sapporo, Hokkaido, 060-8628, Japan

Corresponding author: Osamu Fujita

Division of Mechanical and Space Engineering, Hokkaido University, Kita 13 Nishi 8 Kita-ku, Sapporo, Hokkaido, 060-8628, Japan

TEL: +81-11-706-6385

FAX: +81-11-706-7841

E-mail: ofujita@eng.hokudai.ac.jp

Abstract

Flames propagating in tubes open at the ignition end typically show two different kinds of thermo-acoustic instability namely, primary and secondary. Secondary acoustic instability is accompanied by parametric instability of flame front during which, cellular structures on the flame surface oscillate with half the acoustic frequency of excitation. The growth rates associated with secondary acoustic instability of flame structure are higher compared to primary instability of flames leading to very high peak pressures. In this work we present experimental and theoretical study on parametric instability of downward propagating $C_2H_4/O_2/CO_2$ flames at two different *Le* of 1.0 and 0.8. Lower *Le* mixtures are found to be more unstable. Parametric instability of higher acoustic modes is reported for the first time for gaseous fuels. Higher modes of parametric instability transitioned successively to lower modes as the flame propagated downward. Growth rate of parametric instability is measured in experiments. Theoretical prediction of growth rate is done based on velocity coupling mechanism. Theoretical calculations provide good approximation of growth rates and its variation with frequency.

Keywords: Secondary instability, Downward propagating flames, Combustion tube, Parametric instability, Lewis number, Higher modes

1. Introduction

Thermo-acoustic instability due to coupling of combustor acoustics and unsteady combustion [1], [2] are major challenge for design and operation of combustion devices including gas turbine engines, rocket motors and industrial furnaces. The concern has increased in recent times due to advent of lean premixed combustors designed to meet emission requirements but are prone to instabilities. The criterion governing thermo-acoustic instability had been established by Rayleigh [3] more than a century ago, but the underlying mechanisms has only been investigated from first principles in recent decades. The criterion states that if the integral of product pressure and heat release fluctuations are positive over a cycle, pressure fluctuations would be amplified. A simple experiment to generate thermo-acoustic instability is a downward propagating flame in a tube [4]. Flame when ignited at the top propagates downward and interacts with self-generated acoustics. Two kinds of instability were observed, namely, primary and secondary instability. Primary instability is observed for moderately strong mixtures and primary instability is followed by a secondary instability for sufficiently stronger mixtures, where strength is identified by laminar burning velocity of mixture. Similar observations were reported for flame propagating downward in the annulus between two cylinders [5] [6] [7] [8]. Study on turbulization mechanism [9], onset of primary instability using laser irradiation [10][11][12]and effect of Lewis number [13] [14] [15] have also been studied in downward propagating flame setup. Effect of geometrical parameters on thermo-acoustic instability were also clarified [16].

The simplicity of propagating flames in tubes lies in the fact that the combustible mixture can be quiescent, so, the fluid flow is only due to self-generated acoustics and remains mostly laminar. As it is not a continuous flow experiment, the instabilities due to inlet turbulence and vorticity production at burner inlet are non-existent. The possible mechanism of thermo-acoustic instability is through direct effect of pressure on burning rate (pressure coupling) or change in flame area and burning rate due to action of acoustic velocity and acceleration on premixed flame (velocity coupling). Due to its simplicity it is

amenable to theoretical analysis considering the laminar flame structure in detail through large activation energy asymptotic [17] and provides useful information about these important coupling mechanisms. Pressure coupling mechanism was analyzed theoretically using one-step [18][19] and two-step chemistry [20]. The effect of pressure on premixed flames have also been studied experimentally [21] and numerically [22]. Detailed chemical mechanisms have also been used to study premixed flame -acoustics coupling [23][24]. Velocity coupling was analyzed theoretically, and transfer function was derived for weakly cellular flames [25] based on effect of hydrodynamics and diffusion on premixed flame stability [26]. Nonlinear coupled equations were later derived considering both these mechanisms [27] and later studied for weakly non-linear case [28]. Some aspects of experimental observation e.g. appearance of secondary instability after primary instability were predicted.

A primary instability occurs when a hydrodynamic (D-L) instability of flame front is suppressed by flame-acoustic interaction and sustained pressure oscillations are generated in the process. Growth rates of primary acoustic instability has been measured in experiments and matched within a factor of two with their theoretical predictions based on velocity coupling mechanism with an artificial modification suitable for non-linear cells [29]. Secondary instability is generated by existing primary instability and is accompanied by a parametric instability. Considerably higher growth rates are observed during secondary acoustic instability. The structures on flame front oscillate with half the frequency of acoustic oscillation during the parametric instability. This is similar to Faraday instability. The parametric instability was studied experimentally in a stabilized flame setup and theoretically using laminar flame theory [30]. The wavenumber of flame cells at the onset of parametric instability was well predicted. Analytical solution was developed for parametric instability in the limit of high frequency acoustic oscillations [31]. Parametric instability of flame front in H_2/air mixtures were also studied and the growth rate of parametric instability was presented [32] [33]. The growth rate of parametric instability of structures on flame front is not the same as the growth rate of acoustic pressure amplitude during secondary acoustic instability

observed in downward propagating flame experiments which is also caused by parametric instability. The measurement of growth rates was done in propagating flame in Taylor-Couette combustor [6]. Moreover, there had been no attempts to predict the growth rate of secondary instability. This is the motivation of the present work. The occurrence of sudden high amplitude pressure oscillations in practical combustors can be due to a similar mechanism as secondary instability. However, this aspect is yet to be studied.

The current work presents an experimental and theoretical study of secondary acoustic instability induced by parametric instability of downward propagating flames in tubes. Flame dynamics and effect of Lewis number, *Le* on secondary instability is discussed. Growth rates are measured, and a simple analytical framework is discussed to compute the growth rates.

2. Experimental method

A schematic of the experimental setup is shown in Fig. 1. A transparent acrylic tube of length 70.2 cm and diameter 5.0 cm is fixed vertically to investigate the secondary instability of downward propagating flames. The combustion tube was closed at bottom and a lid was fixed on springs on the upper side which can be opened by the action of an electromagnet. The tube was filled with $C_2H_4/O_2/CO_2$ mixture which was allowed to settle for five minutes. Then, the mixture was ignited at the open end by an electric spark. The spark ignition electrodes were positioned at 7.0 cm from top open end for all the experiments. During the flame propagation from top to bottom, the tube had one end open and another end closed. The downward propagating flame was filmed using a high-speed camera, FASTCAM at 3000 to 5000 frames per second. The pressure fluctuations during flame propagation were measured at sampling rate of 10 kHz using a PCB Piezotronics 106B52 dynamic pressure sensor which was flush-mounted at the bottom of the tube.

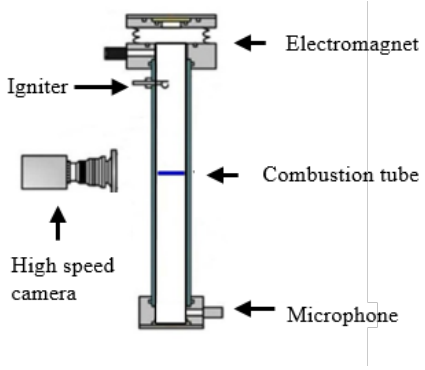

Figure 1. Schematic of experimental setup.

$C_2H_4/O_2/CO_2$ mixture of two equivalence ratios (**Φ)** 0.8 ($Le \approx 1.04$) and 1.2 ($Le \approx 0.80$) was used. This facilitated the study of effect of Lewis number on secondary instability. CO_2 dilution was varied to obtain different laminar burning velocity (S_L) of the fuel/air mixtures at constant equivalence ratios. S_L was calculated with chemical kinetic mechanism of USC II [34] using CHEMKIN Pro. The initial temperature (~300 K) and pressure (1 atm) are at ambient conditions. The mixture compositions used in current work

and respective properties are tabulated in Table 1. **Φ** is equivalence ratio, D is thermal diffusivity of mixture, c is sound speed, ρ is density of mixture. The subscripts 1 and 2 refer to unburnt and burnt mixture conditions.

Table 1. Mixture composition and properties.

Mix.	**C_2H_4 (%)**	**O_2 (%)**	**CO_2 (%)**	**S_L (cm/s)**	**Φ**	**Le**	**D_1 (cm^2/s)**	**D_2 (cm^2/s)**	$\frac{c_1}{c_2}$	$\frac{\rho_1}{\rho_2}$
1	7.16	26.84	66.00	27.54	0.8	1.059	0.134	4.276	0.380	7.022
2	7.35	27.56	65.08	30.00		1.061	0.135	4.421	0.377	7.145
3	7.53	28.25	64.21	32.50		1.062	0.136	4.537	0.374	7.261
4	7.71	28.92	63.37	34.98		1.063	0.136	4.689	0.371	7.367
5	7.88	29.56	62.56	37.50		1.065	0.137	4.815	0.369	7.470
6	8.06	30.21	61.74	40.01		1.066	0.137	4.935	0.367	7.565
7	8.21	30.80	60.99	42.50		1.067	0.138	5.059	0.365	7.654
8	8.38	31.41	60.21	45.00		1.069	0.138	5.159	0.364	7.741
9	8.53	31.99	59.48	47.50		1.07	0.139	5.267	0.362	7.824
10	8.68	32.55	58.77	50.00		1.071	0.139	5.371	0.361	7.902
11	9.15	22.87	67.98	22.53	1.2	0.8	0.131	4.484	0.379	7.332
12	9.42	23.55	67.03	24.98		0.802	0.131	4.675	0.375	7.503
13	9.69	24.23	66.08	27.51		0.804	0.132	4.862	0.372	7.656
14	9.94	24.86	65.20	30.00		0.806	0.133	5.034	0.369	7.799
15	10.20	25.49	64.31	32.51		0.808	0.133	5.201	0.366	7.935
16	10.44	26.09	63.47	35.00		0.81	0.134	5.355	0.364	8.060
17	10.67	26.69	62.64	37.50		0.812	0.134	5.503	0.362	8.176

18	10.89	27.24	61.87	40.00	0.814	0.135	5.642	0.360	8.285
19	11.12	27.79	61.09	42.50	0.815	0.135	5.780	0.358	8.391
20	11.33	28.33	60.34	45.01	0.817	0.135	5.910	0.357	8.489

3. Analytical method

The acoustics in the tube is treated considering the wall losses and radiation loss from the open end of tube following [18]. The spatio-temporal (x, t) pressure and velocity fluctuations can be written as

$$\delta p_{1,2} = \{A_{1,2} \exp(n_{1,2}x) + B_{1,2} \exp(-n_{1,2}x)\} exp(i\omega t) \quad (1)$$

$$\delta u_{1,2} = -\frac{n_{1,2}}{i\omega\rho_{1,2}}\{A_{1,2} \exp(n_{1,2}x) - B_{1,2} \exp(-n_{1,2}x)\}\exp(i\omega t) \quad (2)$$

where

$$n_{1,2} = \frac{i\omega}{c_{1,2}}(1 + \phi_{1,2}) \quad (3)$$

and

$$\phi_{1,2} = \{Pr^{\frac{1}{2}} + \frac{(C_p - C_v)}{(C_p C_v)^{\frac{1}{2}}}\}\frac{D_{1,2}^{1/2}}{R(2\omega)^{1/2}}(1 - i) \quad (4)$$

ω is the circular frequency, $\rho_{1,2}$ is density, $c_{1,2}$ is speed of sound, Pr, Prandtl number, C_p C_v are specific heats, $D_{1,2}$ are thermal diffusivities and R is the radius of the tube. The subscripts 1 and 2 refer to unburnt and burnt sections of the gas. The constants $A_{1,2}$ and $B_{1,2}$ can be eliminated using four boundary conditions. Two boundary conditions at the closed and open ends of tube can be written respectively as

$$\delta u_1 = 0 \text{at } x = -rL \quad (5)$$

and

$$\delta p_2 = K_2 \rho_2 c_2 \delta u_2 \text{ at } x = (1-r)L \tag{6}$$

where,

$$K_2 = \frac{\omega^2 R^2}{2c_2^2} + i\frac{8\omega R}{3\pi c_2} \tag{7}$$

Considering low Mach number assumption, it is assumed that there is no pressure jump across flame front. This can be written as

$$\delta p_1 = \delta p_2 \text{ at } x = 0 \tag{8}$$

The velocity fluctuations across flame front are related by the velocity coupling transfer function, Γ

$$\frac{\delta u_2(0)}{\delta u_1(0)} = (1+\Gamma) \tag{9}$$

After eliminating $A_{1,2}$ and $B_{1,2}$ using boundary conditions from Eqn. 5, 6, 8 and 9, eigen mode equation is obtained as

$$\frac{\rho_2 c_2}{\rho_1 c_1}\frac{(1+\phi_1)}{(1+\phi_2)}\tan\{rX(1+\phi_1)\}\tan\left\{\frac{\ln(K)}{2i} - (1-r)\frac{c_1}{c_2}X(1+\phi_2)\right\}(1+\Gamma) = -1 \tag{10}$$

Here, c is speed of sound; ϕ is wall loss parameter; K is radiation loss parameter; r represents flame position along the length of tube varying from 0 at closed end to 1 at open end; normalized frequency, $X = \frac{\omega L}{c_1}$ and

$$K = \frac{\frac{K_2 c_2 n_2}{i\omega} - 1}{\frac{K_2 c_2 n_2}{i\omega} + 1} \tag{11}$$

The free eigen mode equation, assuming no losses and no velocity coupling (flame as passive surface), can be obtained from eigen mode equation, Eqn. 10 and is written as

$$\frac{\rho_2 c_2}{\rho_1 c_1}\tan\{rX_0\}\tan\left\{(1-r)\frac{c_1}{c_2}X_0\right\} = 1 \tag{12}$$

Calculated values of $\frac{\rho_2}{\rho_1}$ and $\frac{c_2}{c_1}$ are used for each burning velocity. Figure 2 shows first four free eigen modes of the tube for S_L=20 and 50 cm/s for equivalence ratio of 0.8. The frequency is slightly higher for higher burning velocity.

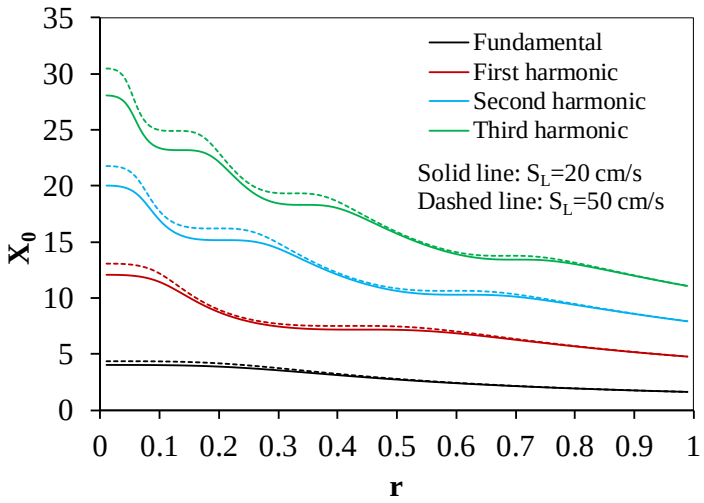

Figure 2. First four free eigen modes of tube computed for S_L= 20 cm/s and 50 cm/s of $C_2H_4/O_2/CO_2$ mixture with equivalence ratio 0.8.

Stability analysis can be performed by expanding Eqn. 10 around the computed free eigen modes of the tube, X_0 obtained by solving Eqn. 12. Substituting, $X = X_0 + \delta X$ in Eq. 10 and treating $\phi_{1,2}$, K as small parameters, so that their higher order terms can be neglected, we obtain for non-dimensional growth rate of linear instability, $-Im(\delta X) = \frac{L}{c_1\tau_{inst}}$

$$\begin{aligned}-Im(\delta X)\{r\left(1+tan^2(rX_0)\right)+(1-r)\frac{\rho_2}{\rho_1}(1+tan^2\left((1-r)\frac{c_1}{c_2}X_0\right)tan^2(rX_0)\} = Im(\Gamma)\tan(rX_0) - \\ \left(tan^2(rX_0)\frac{\rho_2 c_2}{\rho_1 c_1}+\frac{\rho_1 c_1}{\rho_2 c_2}\right)Re(K_2) + Im(\phi_1)\{rX_0\left(1+tan^2(rX_0)\right)+\tan(rX_0)\} + Im(\phi_2)\{(1- \\ r)\frac{c_1}{c_2}X_0\left(tan^2(rX_0)\frac{\rho_2 c_2}{\rho_1 c_1}+\frac{\rho_1 c_1}{\rho_2 c_2}\right)-\tan(rX_0)\}\end{aligned} \tag{13}$$

The instability appears when $Im(\delta X)$ is negative. The theoretical growth rate can be found by evaluating $-Im(\delta X)$ from Eqn. 13. The values of $\frac{\rho_2}{\rho_1}$ and $\frac{c_2}{c_1}$ are noted in Table 1 for each S_L. To find the growth rate, first X_0 is obtained for a given r and S_L by solving Eqn. 12. Corresponding r and X_0 are substituted in Eqn. 13 along with calculated values for $Im(\Gamma)$, $Im(\phi_{1,2})$ and $Re(K_2)$ to find growth rate. The expressions for $Im(\phi_{1,2})$ and $Re(K_2)$ are taken from [18] and depend on diameter and length of tube.

$$-Im(\phi_{1,2}) = 1.74\left(\frac{D_{1,2}}{2Lc_1}\right)^{\frac{1}{2}}\left(\frac{R}{L}\right)^{-1}(X_0)^{\frac{-1}{2}} \tag{14}$$

$$Re(K_2) = 0.5\left(\frac{c_1}{c_2}\right)^2\left(\frac{R}{L}\right)^2(X_0)^2 \tag{15}$$

$D_{1,2}$ is given in Table 1. $c_1 = 26700\ cm/s$ (for CO_2) is used for all the mixtures. c_1 for actual mixture is higher than that for pure CO_2 but use of actual c_1 for each mixture has negligible influence on calculated growth rate.

Finally, we consider the transfer function Γ. Present theoretical analysis of growth rate of secondary acoustic instability of downward propagating flames is based on the velocity coupling mechanism. The velocity coupling transfer function (Γ) for marginally stable cellular flame where $ak \ll 1$ (a is amplitude and k is wavenumber of flame cell) was initially derived by Pelce and Rochwerger [25] to study vibratory instability of flames. Clanet et al. [29] argued that this transfer function can't be used as it is for flames where $ak \approx 1$ and suggested an artificial modification to the transfer function. The modified velocity coupling transfer function was applied to flames where $ak \approx 1$ and utilizes average measured values of wavenumber and amplitude of the cellular flame. Until now, this mechanism has only been used to study the primary acoustic instability and calculate its growth rates. In the primary acoustic instability, a cellular flame when subjected to acoustic fluctuations undergoes flame shape modulation leading to instability. If we consider the secondary instability, a similar mechanism is at work. The flame under primary instability develops corrugations which leads to sudden increase in amplitude of pressure oscillations, possibly

through a similar velocity coupling mechanism. Only difference being that the wavenumbers can be considerably larger than those of primary acoustic instability. Hence, it is possible to study the growth rates of secondary instability using these models. In this work, we consider these two analytical models along with a model used in our last work [16] and compare their predictability. These models are called Model I, Model II and Model III and are described in appendix A.

4. Results and discussion

4.1 Experimental flame regimes

Three flame regimes showing parametric instability of different acoustic modes are observed in current experiments for burning velocity of mixture between 20 cm/s and 50 cm/s with Mix. 1 to 20 from Table 1. These are described here in order. Regime I to IV are described in our previous work [16]. Figure 3 shows representative images at various locations of a downward propagating flame for Regime V for S_L=27.5 cm/s (*Le*=1.0). In regime V, cellular structures are formed on the flame front soon after ignition. The amplitude of flame cells reduces slightly as the flame travels downstream due to primary acoustic instability. Thereafter, highly corrugated structures with deep vibrating cells are formed leading to fluctuating turbulent flame. This is called the secondary instability of flame which is accompanied by high amplitude pressure oscillations. The pressure fluctuations during flame propagation and corresponding FFT analysis are also shown in Fig. 3. The dominant frequency of pressure fluctuation is close to the fundamental mode of the tube (Ideally ~ 100 Hz). As the flame moves downward the average temperature of tube increases which leads to increase in the fundamental frequency. The characteristics of *Le*=0.8 mixtures were similar, but the instability began slightly earlier and at lower S_L compared to *Le*=1.0 case.

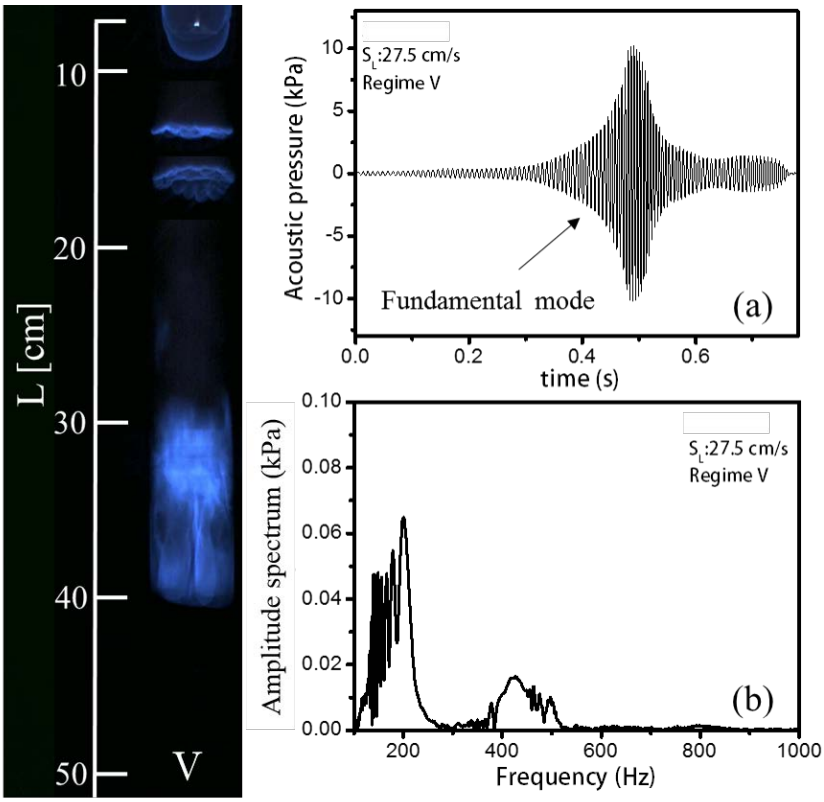

Figure 3. Representative flame images during flame propagation of regime V for Mix. 1 a) pressure fluctuations during flame propagation b) FFT of pressure signal.

Figure 4 shows characteristics of regime VI. In regime VI, instability corresponding to the first harmonic is observed after the flame moves some distance downward after ignition. On visual inspection of flame motion, it was revealed that the flame undergoes parametric instability during the first harmonic instability i.e. the structure on the flame oscillate with half the frequency of acoustic oscillations. Moreover, in some cases, primary instability of fundamental mode is observed just after ignition for a brief time before first harmonic instability sets in. Thereafter, the first harmonic instability decreases, and flame undergoes a silent phase with minimal instability. Soon, the corrugations develop on flame and a secondary instability corresponding to fundamental mode is observed, similar to regime V. For *Le*=0.8, the transition generally happened sooner. The pressure fluctuation time history clearly shows two different phases of instability. It can also be seen that maximum pressure amplitude corresponding to fundamental mode parametric

instability is higher than that of first harmonic instability. Two characteristic frequencies corresponding to fundamental and first harmonic modes can be clearly observed from the FFT analysis of pressure time history.

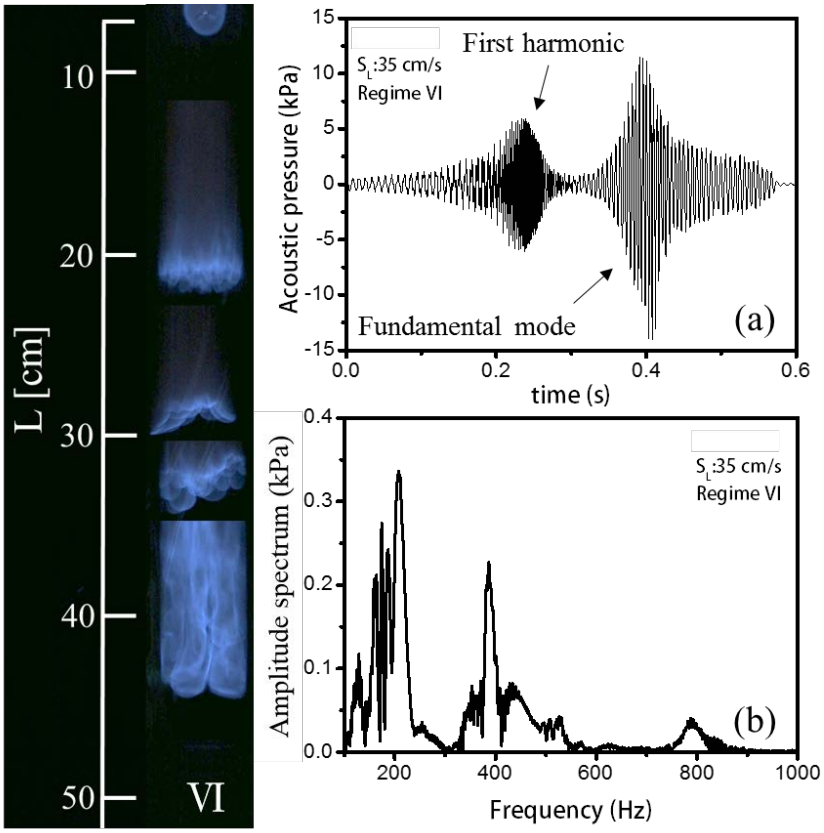

Figure 4. Representative flame images during flame propagation of regime VI for Mix. 4 a) pressure fluctuations during flame propagation b) FFT of pressure signal.

Figure 5 shows characteristics of regime VII. Flame undergoes primary instability as soon as it is ignited. As the flame moves down, an instability corresponding to second harmonic is observed. This instability is also parametric in nature. After that the instability transitions into a first harmonic instability which later transition into a fundamental mode parametric instability. The flame images show the representative flame images of various stages discussed here. Pressure time history also shows three different phases of instability corresponding to first three modes of tube. The transition from one mode of instability to

another is not so smooth and it was found on many occasions that pressure fluctuations of different modes exist simultaneously.

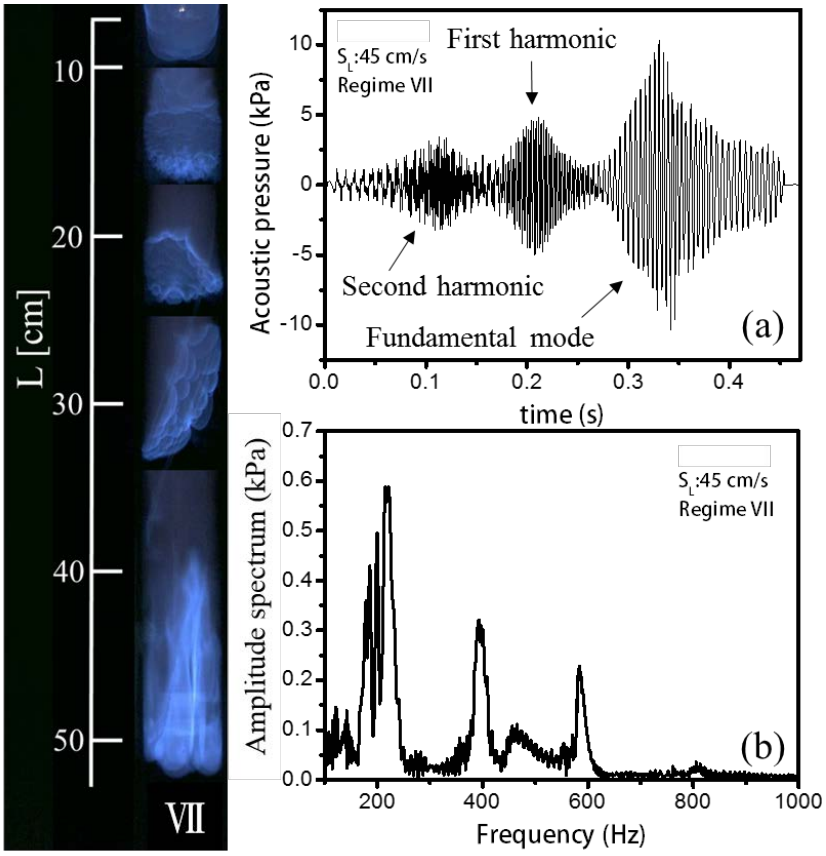

Figure 5. Representative flame images during flame propagation of regime VII for Mix. 8 a) pressure fluctuations during flame propagation b) FFT of pressure signal.

FFT analysis of pressure time history shows the frequency corresponding to first three acoustic modes for a tube closed at one end and open at another. On a first look it appears that the frequencies are f:2 f:3 f, (f is fundamental frequency) while it should be f:3 f:5 f, which is appropriate for an open-closed tube. This can be explained by understanding that the natural frequency increases as the flame moves downstream. As second harmonic is closest to the open end the frequency is close to 600 Hz which is five times of natural frequency of around 120 Hz. First harmonic is observed at more downward location at

around 400 Hz which is three times of natural frequency of around 130-140 Hz at that location. So, the frequencies observed do correspond to first three harmonics of the tube.

The pressure fluctuations of regime VI and VII are consistent with the growth rates of instability shown in Fig. 11 or 12 (Appendix A). The growth rate of higher modes peak closer to the open end. Thus, second harmonic occurs first in regime VII and as the flame travels towards closed end first harmonic and fundamental mode instability occurs. Flame responses similar to regime VI and VII were earlier reported by Clanet et al. [29] for *n*-decane spray flames but were not observed for gaseous propane flames of similar S_L as in current work. They noted that the higher harmonics became unstable in spray flames owing to a different mechanism related to difference in motion of gaseous molecules and fine fuel droplets which leads to stronger instability. However, current experiments show that these regimes can also be observed for gaseous fuel flames. There are two possible reasons for this observation. First, the diameter of tube used in current work (5.0 cm) is lower (10.0 cm) compared to that in [29]. Smaller diameter leads to stronger instability as was shown in our earlier work [16]. Second, CO_2 dilution is used in current work compared to N_2 dilution in [29] for similar S_L. It may appear counterintuitive at first that CO_2 dilution also leads to stronger instability because CO_2 is usually added to enhance flame stability and eliminate flashback [35]. The stabilizing effect is due to reduction in flame temperature and S_L [36]. However, here we compare CO_2 and N_2 dilution cases at similar S_L. To get same S_L of 35 cm/s for C_2H_4 at equivalence ratio of 0.8, CO_2/O_2 mole ratio is 2.19 but N_2/O_2 ratio is 4.47 (In air, N_2/O_2 ratio is 3.76). This means that CO_2 dilution required is much less compared to N_2 dilution if we keep S_L constant. We can check from Table 1 that molar ratio of CO_2 in mixture decreases as we increase S_L. Hence at higher S_L the CO_2 dilution is even less. Of course, if we keep same diluent/O_2 ratio CO_2 diluted mixture will have much lower flame temperature and burning velocity and thus very low instability compared with N_2 diluted mixture. Due to lower dilution in case of CO_2 diluted mixture for same S_L, CO_2 diluted mixture will have

higher adiabatic flame temperature than N_2 diluted mixture. This will lead to higher coupling constant and thus higher instability [13].

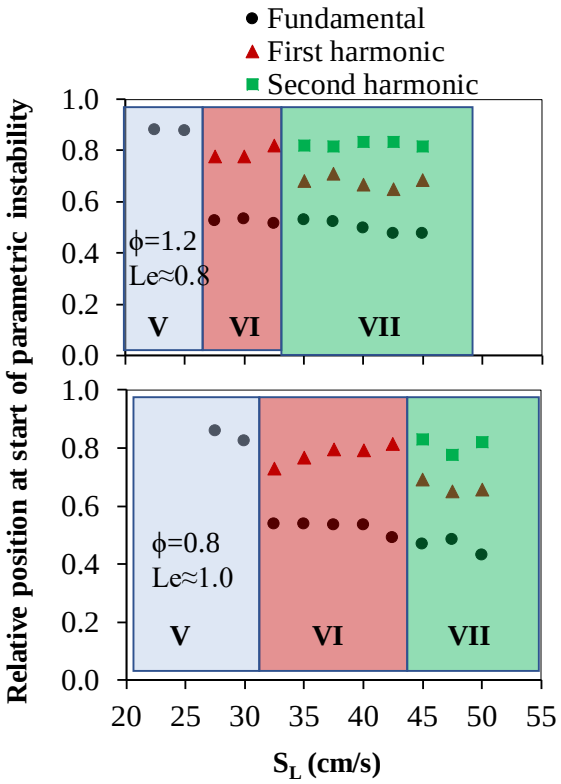

Figure 6. Overall flame responses for Mix. 11-20 from Table 1 (**Φ** = 1.2, *Le*=0.8) (top) and Mix. 1-10 from Table 1 (**Φ** = 0.8, *Le*=1.0) (bottom). Relative position at onset of instability of various modes are also shown.

The mixtures with *Le*=0.8 (Mix. 11-20 from Table 1) also show similar flame responses. Figure 6 shows effect of S_L on the flame regimes observed for two different *Le* mixtures. As the S_L is increased the flame regimes change from V to VI to VII. Effect of *Le* can be clearly observed. Low *Le* mixtures show stronger instability as the S_L at the onset of regime VI and VII are lower than that for *Le*=1.0 mixture.

Searby and Rochwerger [30] noted that the parametric instability of the flame can be the reason for high amplitude pressure oscillations in downward propagating flames. However, it has not been clearly proven yet. Here, we provide a conclusive evidence of the fact that parametric instability of flame leads to higher

growth rate and large amplitude pressure fluctuations. Figure 7 shows measured growth rate before and after the onset of parametric instability. Only fundamental mode data is considered. It can be clearly seen that the growth rate increases significantly after the onset of parametric instability. The increase in growth rate is around ten to fifteen times for regime V. For regime VI and VII the growth rate increases around two-fold.

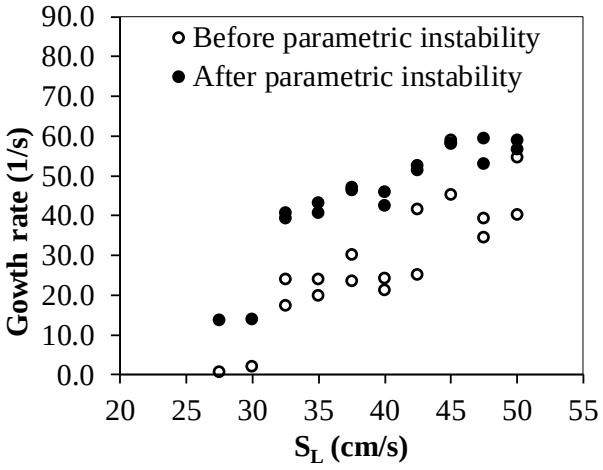

Figure 7. Measured growth rates before and after the onset of parametric instability of fundamental mode for Mix. 1-10 from Table 1($\boldsymbol{\Phi}$ =0.8).

4.2 Growth rates: Effect of Lewis number

Growth rates of secondary acoustic instability was measured for two different *Le* mixtures at various burning velocities of employed mixtures and are shown in Fig. 8 for first three modes. The horizontal axis, ωτ denotes ratio of chemical time scale, $\tau = \frac{D_1}{S_L^2}$, to acoustic time scale $\frac{1}{\omega}$. Here, ω is circular frequency, $2\pi f$, f, being the measured frequency. To get the measured frequency, FFT is done of pressure signal in duration $t \pm 0.04$ s, t is the time when parametric instability is generated for each mode. So, this frequency contains the effect of position along the tube at which the parametric instability is generated for each mode. The growth rate is measured using the pressure time history. Clanet et al. [29] use the equation $p = A \exp\left(\frac{t}{\tau_{ins}}\right) \cos(\omega t + \varphi)$ to fit their pressure time history, here $\frac{1}{\tau_{ins}}$ is the growth rate of instability. The

frequency in their work is constant. It is understandable, as, during the primary instability the frequency doesn't increase much. But, during secondary instability the frequency changes significantly because the increase in flame area is much higher compared to primary instability leading to larger temperature change and thus acoustic frequency. So, in our work, we take the envelope of amplitudes of pressure fluctuations and fit an exponential curve $p = A \exp\left(\frac{t}{\tau_{ins}}\right)$ to find the growth rate.

Generally, with increase in ωτ, growth rate decreases. Similar result was also observed by Clanet et al. [29]. For every mode of instability, the lower *Le* leads to higher growth rates. Lower than unity *Le* leads to lower *Ma* compared to *Le*=1 which means slightly higher growth rate as can be seen from Fig. 11 (Appendix A). The flame cells are convex towards the unburnt gas, thus owing to *Le* effect, focusing of heat flux occurs increasing the effective flame temperature and thus the instability. It is also apparent that with increase in mode of the instability, the *Le* effect is more significant.

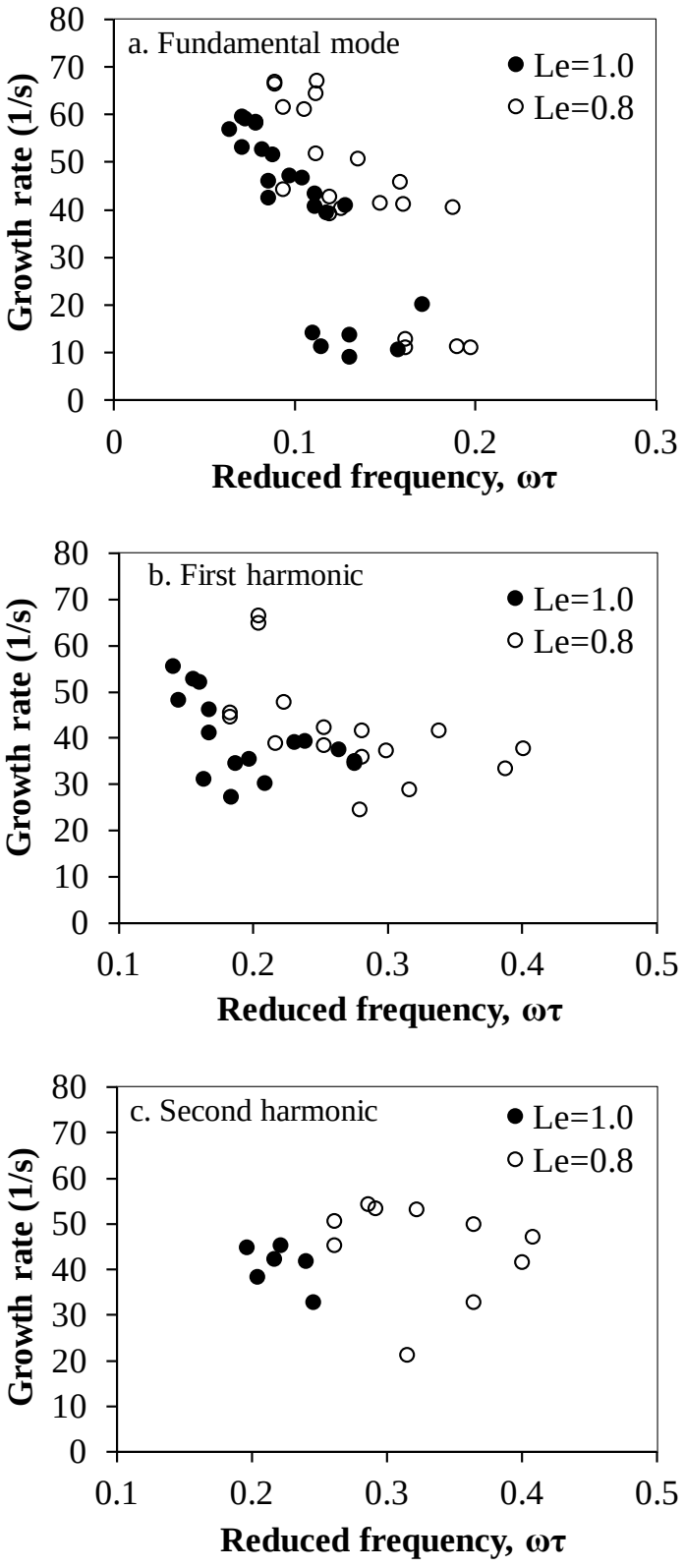

Figure 8. Effect of Lewis number on growth rate of secondary instability a. fundamental mode b. first harmonic c. second harmonic. *Le*=1.0, Mix. 1-10. *Le*=0.8, Mix. 11-20.

4.3 Growth rates: comparison between experiments and theory

In this section, we compare growth rates of secondary instability with their theoretical predictions based on velocity coupling. Before that we discuss the measurement of wavenumber and amplitude of flame cells and associated difficulties. The measurement of position of onset of instability along with amplitude and wavenumber is quite complicated, particularly at higher burning velocity where higher harmonics are observed. The flame brush length at the onset is not small in many cases. Also, not all flame cells go through the parametric instability because at the present conditions, hydrodynamic and parametric instability co-exist [30]. The flame cells most downward are more susceptible to instability and that is where the instability begins and flame cells in upward location catchup later during the instability cycle. The observed growth rate is due to combined effect of all the flame cells undergoing parametric instability over a time.

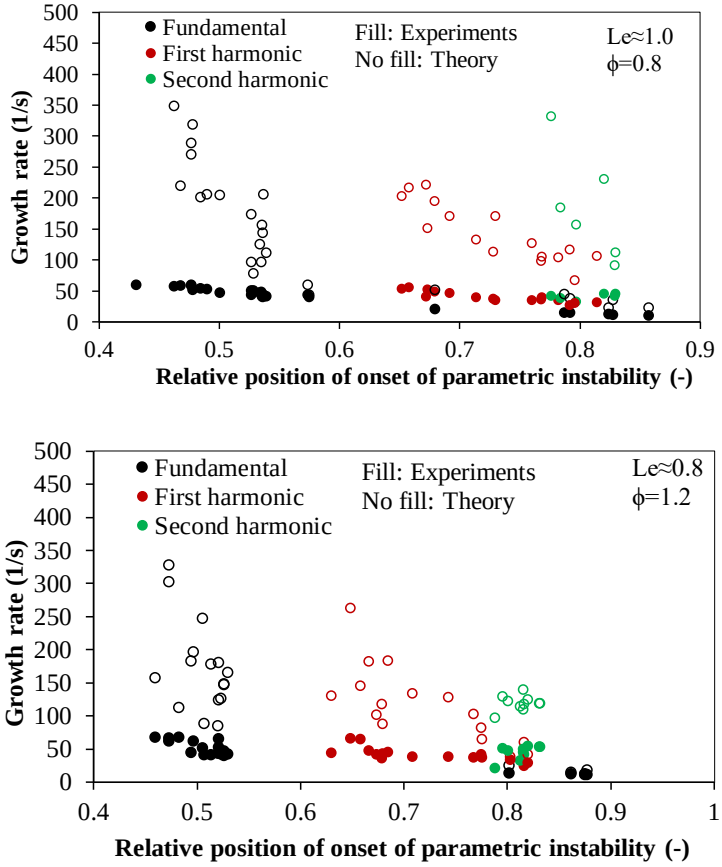

Figure 9. Measured and predicted growth rates for first three harmonics.

Figure 9 shows the measured and theoretical growth rates as a function of flame position at the onset of parametric instability along the tube for *Le*=1.0 and *Le*=0.8 mixtures. The position of onset of instability is taken as the position of flame tip at the onset. So, the calculated growth rate indicates upper limit of the growth rate. Both, experimental and theoretical growth rate increases as the onset position of instability shifts down the tube. The qualitative behavior of growth rates is very well predicted which could suggest that velocity coupling mechanism with linear theory can predict major characteristics of secondary instability growth rate. However, the theoretical predictions generally overestimate the growth rate. There are two possible reasons for such overestimation. First, the unmeasured cells and errors in measurement of cell sizes due to unclear transition between regimes could affect the average cell parameters used in calculation. Second, it might be possible that the non-linearities associated with larger cell sizes at $ak>1$ induce lower growth rates than that predicted by the linear model. However, an order of magnitude estimate is still predicted. When the flame brush thickness is larger the discrepancy is larger. Despite this, the predictions of linear model cannot be undermined as the qualitative characteristics of complex behavior of secondary instability is still predicted within a factor of five as can be seen from Fig. 10.

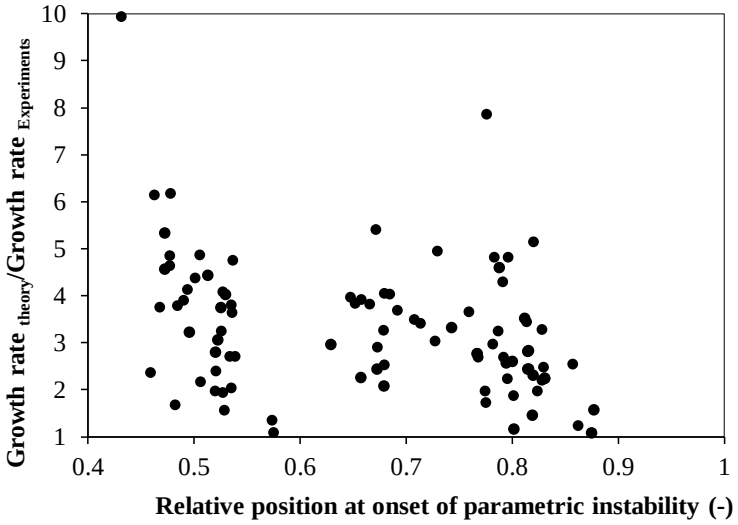

Figure 10. Ratio between computed and measured growth rates of parametric instability

Conclusions

Secondary instability of downward propagating flames was studied experimentally and analytically for two different *Le*. Parametric instability of higher harmonics was observed for the first time for gaseous fuel flames. Lower *Le* leads to stronger instability. The occurrence of parametric instability was shown to be the reason for increase in growth rates leading to secondary acoustic instability with high amplitude pressure oscillations. Velocity coupling mechanism can be successfully used to calculate the measured growth rates of secondary thermo-acoustic instability in a combustion tube.

Acknowledgements

This study is carried out under the collaboration of Hokkaido University and Mitsubishi Heavy Industries. The analytical part of this study was carried out under support of a Grant-in-Aid for Scientific Researches (KIBAN (B) #26289042 and KIBAN(A)#18H03755) from MEXT Japan.

Appendix A

Model I

This model is the simplest and was originally derived by Pelce and Rochwerger [25] for flames with $ak \ll 1$. However, to be applicable to current flames, this assumption is relaxed, and the wavenumbers and amplitude of flame structures used in the definition of transfer function and related functions are taken from the experimental measurements

$$\Gamma = \frac{1}{2}\left(\frac{\rho_1 - \rho_2}{\rho_2}\right)(ak)^2 \frac{iC(kd)}{A(kd)\Omega - iB(kd)} \tag{146}$$

The functions $A(kd)$, $B(kd)$ and $C(kd)$ are given as follows adopted from [25]

$$\mathrm{A}(kd) = (2-\gamma) + \gamma kd\{Ma - \frac{1}{\gamma}\ln\left(\frac{1}{1-\gamma}\right)\} \tag{17}$$

$$\mathrm{B}(kd) = 2kd + 2\frac{(kd)^2}{1-\gamma}\{Ma - \ln\left(\frac{1}{1-\gamma}\right)\} \tag{158}$$

$$\mathrm{C}(kd) = \gamma kd[1 - kd\left(Ma - \frac{1}{\gamma}\ln\left(\frac{1}{1-\gamma}\right)\right)] \tag{19}$$

Here, d is flame thickness, $\gamma = \frac{\rho_1 - \rho_2}{\rho_1}$, Ma is Markstein number. These functions are defined assuming that product of density and diffusivity is independent of temperature.

Model II

In this model, the term D is retained in the transfer function which otherwise vanishes for marginally stable flames.

$$\Gamma = \frac{1}{2}(\frac{\rho_1 - \rho_2}{\rho_2})(ak)^2 \frac{i\Omega C(kd)}{A(kd)\Omega^2 - i\Omega B(kd) - D(kd)} \tag{2016}$$

The expressions for $A(kd)$, $B(kd)$ and $C(kd)$ are same as model I and the expression for $D(kd)$ is given as following

$$\mathrm{D}(kd) = \frac{\gamma kd}{Fr}\left[1 - kd\left(Ma - \frac{1}{\gamma}\ln\left(\frac{1}{1-\gamma}\right)\right)\right] - \frac{\gamma}{1-\gamma}[(kd)^2 - (kd)^3\{1 + \frac{\gamma+2}{\gamma}Ma - \frac{2}{\gamma}\ln\left(\frac{1}{1-\gamma}\right)\}] \tag{21}$$

Here, Fr is Froude number defined as $\frac{S_L^2}{gd}$, g is gravitational acceleration taken as 980 cm/s^2.

Model III

This model was proposed by Clanet et al. [29] by artificial modification of model I and it was demonstrated that it predicted for growth rate of primary instability within an order of magnitude for flames with $ak \approx 1$. The expression for transfer function is same as model II but the functions $A(kd)$, $B(kd)$, $C(kd)$ and $D(kd)$ are defined considering temperature dependence of product of density and diffusivity [29] and given as following

$$\mathrm{A}(kd) = (2-\gamma) + \gamma kd(Ma - \frac{J}{\gamma}) \tag{22}$$

$$\mathrm{B}(kd) = 2kd + 2\frac{(kd)^2}{1-\gamma}(Ma - J) \tag{23}$$

$$\mathrm{C}(kd) = \gamma kd[1 - kd\left(Ma - \frac{J}{\gamma}\right)] \tag{24}$$

$$\mathrm{D}(kd) = \frac{\gamma kd}{Fr}\left[1 - kd\left(Ma - \frac{J}{\gamma}\right)\right] - \frac{\gamma}{1-\gamma}[(kd)^2 - (kd)^3\{h_b + \frac{\gamma+2}{\gamma}Ma - \frac{2J}{\gamma} + (2Pr-1)\int_0^1 \big(h_b - h(\theta)\big)d\theta\}\,] \tag{25}$$

Here, $\theta = \frac{T-T_1}{T_2-T_1}$, is the normalized temperature, $h(\theta) = \frac{(\rho D)_\theta}{(\rho D)_{\theta=0}}$, h_b is $h(\theta)$ in burnt gas and

$$\mathrm{J} = \frac{\gamma}{1-\gamma}\int_0^1 \frac{h(\theta)}{1+\theta\frac{\gamma}{1-\gamma}}d\theta \tag{26}$$

Now, $Im(\Gamma)$ needed to calculate the growth rate from Eqn. 13 can be easily shown for model I to be

$$Im(\Gamma) = \frac{1}{2}(\frac{\rho_1-\rho_2}{\rho_2})(ak)^2\frac{\Omega C(kd)A(kd)}{\{A(kd)\Omega\}^2 + \{B(kd)\}^2} \tag{27}$$

And for model II and III to be

$$Im(\Gamma) = \frac{1}{2}(\frac{\rho_1-\rho_2}{\rho_2})(ak)^2\frac{\Omega C(kd)\{A(kd)\Omega^2 - D(kd)\}}{\{A(kd)\Omega^2 - D(kd)\}^2 + \{\Omega B(kd)\}^2} \tag{28}$$

Markstein number can be evaluated using the theoretical expression in Searby and Rochwerger [30]. It was found that *Ma* varied between 4.8 and 6.2 for *Le*=1.0 and between 4.3 and 4.6 for *Le*=0.8. However, the theoretical growth rate is not so sensitive to *Ma* value as can be seen from Fig. 11. It is not to say that

Ma has no effect on growth rate of instability. Effects of *Ma* or *Le* can also be contained in the measured values of amplitude and wavenumber of cellular flames. Hence, in current work, we use values of *Ma*=5.5 for equivalence ratio 0.8 (*Le*=1.0) and *Ma*=4.5 for equivalence ratio of 1.2 (*Le*=0.8) for simplicity.

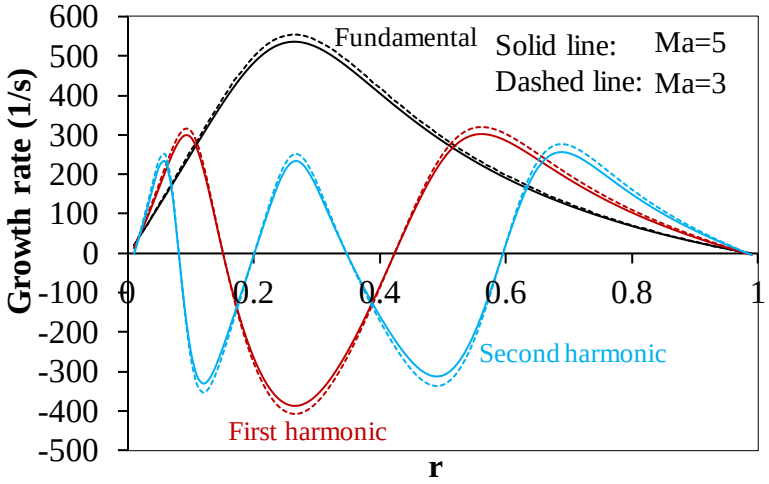

Figure 11. Effect of *Ma* on growth rate of first three harmonics calculated using model I for same value of ak; S_L=47.5 cm/s, Mix 9.

Figure 12 shows comparison among models for growth rate prediction of first three harmonics. Comparing, model I and model II shows the effect of retaining the term D and comparing model II and model III shows the effect of using temperature dependent diffusivities. Retaining the term D leads to slightly smaller growth rates but the effect reduces at higher harmonics. Slightly higher growth rates are found if temperature dependence of diffusivities is considered. Computing growth rates from model III is complicated compared to model I or II as it requires computation of various integrals and knowledge of temperature dependence of diffusivities. Diffusivity and density of unburnt mixture as a function of temperature is calculated using CHEMKIN. The maximum difference among models is around 5%. The most important factor turns out to be the amplitude and wavenumber of flame cells at onset of instability. The inclusion of additional complexity in Model III has no clear advantage over other simpler models

considering that the theoretical model overpredict the growth rate of parametric instability (as presented in section 4.2) and the theoretical models are only approximate at the conditions where $ak \approx 1$.

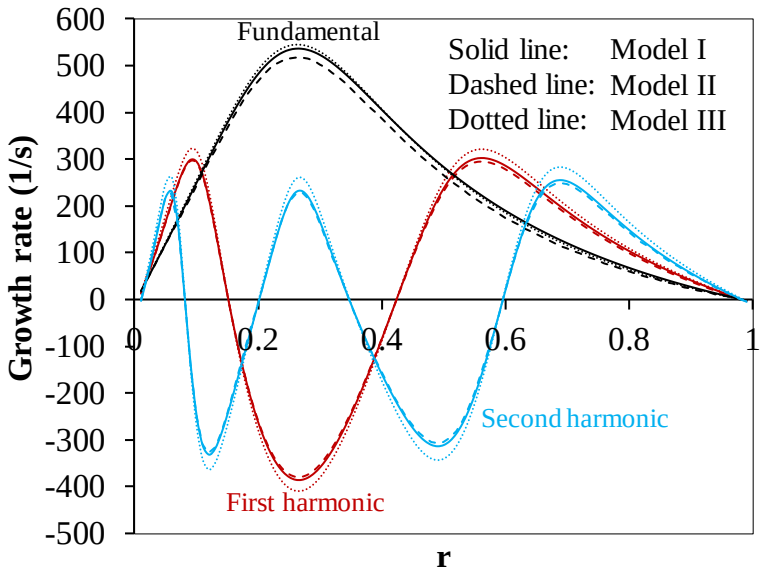

Figure 12. Comparison among models for growth rate of first three harmonics; S_L=47.5 cm/s, Mix 9.

References

[1] T. C. Lieuwen, *Unsteady Combustor Physics*, (2012) . Cambridge: Cambridge University Press, 2012.

[2] T. Poinsot, Prediction and control of combustion instabilities in real engines, Proc. Combust. Inst., 36 (2017) , 1–28.

[3] J. W. S. B. Rayleigh, The explanation of certain acoustical phenomena 1, Nature, 18 (1878) , 319–321.

[4] G. Searby, Acoustic Instability in Premixed Flames, Combust. Sci. Technol., 81 (1992) , 221–231.

[5] V. Vaezi, R. . Aldredge, Laminar-flame instabilities in a taylor-couette combustor, Combust. Flame, 121 (2000) , 356–366.

[6] R. C. Aldredge, N. J. Killingsworth, Experimental evaluation of Markstein-number influence on thermoacoustic instability, Combust. Flame, 137 (2004) , 178–197.

[7] V. Vaezi and R. C. Aldredge, Influences of Acoustic Instabilities on Turbulent-Flame Propagation, Exp. Thermal Fluid Sci., 20 (2000), 162-169.

[8] R. C. Aldredge, Methane-Air Markstein Numbers From Measurements Of Thermoacoustic Instability, Combust. Sci. Technol., 177 (2005), 1023-1047.

[9] Y. Taniyama, O. Fujita, Initiation and formation of the corrugated structure leading to the self-turbulization of downward propagating flames in a combustion tube with external laser absorption, Combust. Flame, 161 (2014) , 1558–1565.

[10] S. H. Yoon, T. J. Noh, O. Fujita, Onset mechanism of primary acoustic instability in downward-

propagating flames, Combust. Flame, 170 (2016) , 1–11.

[11] M. Tsuchimoto, O. Fujita, T. Honko, Y. Nakamura, H. Ito, Research on the relation of flame front curvature and oscillatory flame propagation by external laser irradiation method, Proc. Combust. Inst., 32 (2009) , 1003–1009.

[12] J. S. Park, O. Fujita, Y. Nakamura, H. Ito, Transition of flat flames to turbulent motion induced by external laser irradiation, Proc. Combust. Inst., 33 (2011) , 1105–1112.

[13] S. H. Yoon, T. J. Noh, O. Fujita, Effects of Lewis number on generation of primary acoustic instability in downward-propagating flames, Proc. Combust. Inst., 36 (2017) , 1603–1611.

[14] S. H. Yoon, L. Hu, O. Fujita, Experimental observation of pulsating instability under acoustic field in downward-propagating flames at large Lewis number, Combust. Flame, 188 (2018) , 1–4.

[15] Y. Chung, O. Fujita, N. Hashimoto, Effect of Le on criteria of transition to secondary acoustic instability of downward-propagating flame in a tube with controlled curvature induced by external laser, Proc. Combust. Inst., 37 (2019) 1887-1894.

[16] A. K. Dubey, Y. Koyama, N. Hashimoto, O. Fujita, Effect of geometrical parameters on thermo-acoustic instability of downward propagating flames in tubes, Proc. Combust. Inst., 37 (2019) 1869–1877.

[17] P. Clavin, Dynamic behavior of premixed flame fronts in laminar and turbulent flows, Prog. Energy Combust. Sci., 11 (1985) , 1–59.

[18] P. Clavin, P. Pelcé, L. He, One-dimensional vibratory instability of planar flames propagating in tubes, J. Fluid Mech., 216 (1990) , 299–322.

[19] A. C. Mcintosh, Pressure disturbances of Different Length Scales Interacting with Conventional Flames, Combust. Sci. Technol., 75 (1991) , 287–309.

[20] P. Clavin, G. Searby, Unsteady response of chain-branching premixed-flames to pressure waves, Combust. Theory Model., 12 (2008) , 545–567.

[21] A. Wangher, G. Searby, J. Quinard, Experimental investigation of the unsteady response of premixed flame fronts to acoustic pressure waves, Combust. Flame, 154 (2008) , 310–318.

[22] O. J. Teerling, A. C. Mcintosh, J. Brindley, V. H. Y. Tam, Premixed flame response to oscillatory pressure waves, Proc. Combust. Inst., 30 (2005) , 1733–1740.

[23] C. Jiménez, J. Quinard, J. Graña-Otero, H. Schmidt, G. Searby, Unsteady response of hydrogen and methane flames to pressure waves, Combust. Flame, 159 (2012) , 1894–1908.

[24] G. Beardsell, G. Blanquart, Impact of pressure fluctuations on the dynamics of laminar premixed flames, Proc. Combust. Inst., 37 (2019), 1895-1902 .

[25] P. Pelcé, D. Rochwerger, Vibratory instability of cellular flames propagating in tubes, J. Fluid Mech., 239 (1992) , 293–307.

[26] P. Pelce, P. Clavin, Influence of hydrodynamics and diffusion upon the stability limits of laminar premixed flames, J. Fluid Mech., 124 (1982) , 219–237.

[27] X. Wu, M. Wang, P. Moin, N. Peters, Combustion instability due to the nonlinear interaction between sound and flame, J. Fluid Mech., 497 (2003), 23-53.

[28] R. C. Assier, X. Wu, Linear and weakly nonlinear instability of a premixed curved flame under the influence of its spontaneous acoustic field, J. Fluid Mech, 758 (2017) , 180–220.

[29] C. Clanet, G. Searby, P. Clavin, Primary acoustic instability of flames propagating in tubes: cases of spray and premixed gas combustion, J. Fluid Mech., 385 (1999) , 157–197.

[30] G. Searby, D. Rochwerger, A parametric acoustic instability in premixed flames, J. Fluid Mech., 231 (1991) , 529–543.

[31] V. Bychkov, Analytical scalings for flame interaction with sound waves, Phys. Fluids, 11 (1999) , 3168–3173.

[32] J. Yáñez, M. Kuznetsov, R. Redlinger, The acoustic–parametric instability for hydrogen–air mixtures, Combust. Flame, 160 (2013) , 2009–2016.

[33] J. Yáñez, M. Kuznetsov, J. Grune, Flame instability of lean hydrogen-air mixtures in a smooth open-ended vertical channel, Combust. Flame, 162 (2015), 2830-2839.

[34] H. Wang, X. You, A. V. Joshi, S. G. Davis, A. Laskin, F. Egolfopoulos, C. K. Law, USC Mech Version II. High-Temperature combustion reaction model of H2/CO/C1-C4 compounds, http://ignis.usc.edu/USC_Mech_II.htm, May 2007.

[35] J. Lewis, R. Marsh, A. Valera-Medina, S. Morris, H. Baej, The Use of CO_2 to Improve Stability and Emissions of an IGCC Combustor, ASME Turbo Expo 2014: Turbine Technical Conference and Exposition, Düsseldorf, Germany (June 2014) , Paper No. GT2014-25446.

[36] H. Kobayashi, H. Hagiwara, H. Kaneko, Y. Ogami, Effects of CO_2 dilution on turbulent premixed flames at high pressure and high temperature, Proc. Combust. Inst., 31 (2007) , 1451–1458.